High-Dimensional Atomistic Neural Network Potential to Study the Alignment-Resolved O2 Scattering from Highly Oriented Pyrolytic Graphite

Alejandro Rivero Santamaría, Maximiliano Ramos, Maite Alducin, Heriberto Fabio Busnengo, Ricardo Díez Muiño, J. Iñaki Juaristi

High-Dimensional Atomistic Neural Network Potential to Study the Alignment-Resolved O_2 Scattering from Highly Oriented Pyrolytic Graphite.

Alejandro Rivero Santamaría,[*,†,‡] Maximiliano Ramos ,[*,¶,§] Maite Alducin,[*,†,‡] Heriberto Fabio Busnengo,[*,¶] Ricardo Díez Muiño,[*,†,‡] and J. Iñaki Juaristi[*,‖,†,‡]

†*Centro de Física de Materiales CFM/MPC (CSIC-UPV/EHU), Paseo Manuel de Lardizabal 5, 20018 Donostia-San Sebastián, Spain*

‡*Donostia International Physics Center DIPC, Paseo Manuel de Lardizabal 4, 20018 Donostia-San Sebastián, Spain*

¶*Instituto de Física Rosario, CONICET and Universidad Nacional de Rosario, Bv. 27 de Febrero 210 bis, 2000 Rosario, Argentina.*

§*Facultad de Ciencias Exactas, Ingeniera y Agrimensura, Universidad Nacional de Rosario, Av. Pellegrini 250, S2000BTP Rosario, Argentina*

‖*Departamento de Polímeros y Materiales Avanzados: Física, Química y Tecnología, Facultad de Químicas, Universidad del País Vasco (UPV/EHU), Apartado 1072, 20080 Donostia-San Sebastián, Spain*

E-mail: arivero@dipc.org; ramos@ifir-conicet.gov.ar; maite.alducin@ehu.eus; busnengo@ifir-conicet.gov.ar; rdm@ehu.eus; josebainaki.juaristi@ehu.eus

Abstract

A high dimensional and accurate atomistic neural network potential energy surface (ANN-PES) that describes the interaction between one O_2 molecule and a highly oriented pyrolitic graphite (HOPG) surface has been constructed, using the open source package aenet. The validation of the PES is performed by paying attention to static characteristics as well as by testing its performance in reproducing previous ab initio molecular dynamics simulation results. Subsequently, the ANN-PES is used to perform quasiclassical molecular dynamics calculations of the alignment dependent scattering of O_2 from HOPG. Results are obtained for 200 meV O_2 molecules with different initial alignments impinging with a polar incidence angle respect to the surface normal of 22.5° on a thermalized (110 and 300 K) graphite surface. The choice of these initial conditions in our simulations is made in order to perform comparisons to recent experimental results on this system. Our results show that the scattering of O_2 from the HOPG surface is a rather direct process, that the angular distributions are alignment dependent, and that the final translational energy of end-on molecules is around 20% lower than that of side-on molecules. Upon collision with the surface, the molecules initially aligned perpendicular to the surface become highly rotationally excited, whereas a very small change in the rotational state of the scattered molecules is observed for the initial parallel alignments. The latter confirms the energy transfer dependence on the stereodynamics for the present system. The results of our simulations are in overall agreement with the experimental observations regarding the angular distributions shape and the alignment dependence of the in-plane reflected molecules.

1 Introduction

The interaction of O_2 with graphite surfaces has been used as a model for understanding the behavior of carbon-based materials in different applications, such as, processes of burning phenomena in nature, coal gasification, reactions at nuclear reactor walls, and the degradation mechanism of the spacecraft vehicles shielding, among others. In this respect, several experimental[1–5] and theoretical[6–14] studies focused on the interaction of O_2 with highly oriented pyrolytic graphite (HOPG) have been performed. Particularly interesting, among the latest publications on this system, is the

first experimental results on alignment-resolved O_2 scattering from HOPG published by Kurahashi et al.[15] The authors report a marked alignment dependence of the scattering features associated mainly with the surface roughness seen by the scattered molecule. This work is part of the growing interest that the interaction of aligned molecules with surfaces is receiving in the last few years.[15–22] It is thanks to the tremendous advances in experimental setups that it is now possible to know how the stereochemistry and spin state of molecules influence the interaction dynamics and reactivity on different surfaces.

Recently and in order to contribute to the theoretical understanding of the observations by Kurahashi et al,[15] some of us have published a theoretical study[23] using ab initio molecular dynamics (AIMD) calculations on the O_2-HOPG system. The use of AIMD allowed us to describe with accuracy the molecule-surface interaction and obtain new information about the effect of the alignment of the impinging O_2. Even if the alignment of the molecular axis of the side-on molecules in our simulations[24] was not exactly the same one used in the experiments (see below), the results were meaningful to understand the experimental observations regarding the alignment dependence of the in-plane scattering probabilities and the energy loss of the reflected molecules. In particular, the AIMD simulations showed that molecules initially aligned parallel to the surface are more likely to scatter in plane than those initially aligned perpendicular to the surface. Additionally, we found that the final translational energy of end-on molecules was around 10% lower than that of side-on molecules.

The great advantage of having used AIMD was that there was no need to obtain first a continuous representation of the potential energy surface (PES) because the energies and forces during the dynamics are determined on the fly at the density functional theory (DFT) level. In addition, AIMD allows to treat both the molecular and surface atom degrees of freedom (DOF) on equal footing without adding difficulties to the modelization, as compared to traditional simulations in which only molecular DOFs were considered.[25–38] However, it is well known that the main shortcoming of AIMD is the statistical accuracy, due to its computational cost. The limited number of trajectories that can be performed and the restriction in the initial conditions that must be imposed

to simulate the experiments, make it difficult to determine accurately some dynamical quantities, for example, to elucidate small shifts in computed angular scattering distributions and to obtain, with better precision, the amount of energy exchange in the collision process.

In the last few years the irruption of machine learning (ML) algorithms has allowed to construct analytic high dimensional PESs (HD-PESs), that based in atomistic neural networks (ANN),[39] have been used to perform molecular dynamics (MD) studies taking into account all the DOF of the system.[40–47] This approach has a considerably smaller computational cost than AIMD, allowing for a higher statistical accuracy of the results. The ANN-PES concept was developed by Behler and Parrinello[39] in 2007 with the aim to obtain DFT-based PESs without losing the accuracy of the DFT results itself and capable of describing all types of bonding. The main concept in this model was the representation of the total energy of the system as the sum of the energy contributions from each atom depending of its chemical environment. The atomic individual energy is obtained using continuous and differentiable mathematical functions,[39,43,48–54] so-called atomic environment descriptors, that form a vector that is used as input layer of the neural network of the corresponding atom. They are defined within a sphere centered on the atom position, and of radius (R_c). The descriptor vector introduced by Behler and Parrinello[39] to describe the chemical environment of each atom is defined in such a way that results invariant under symmetry operations of the full system, e.g., rotations, translations, and permutations of equivalent atoms.

This work is focused in the development of an ANN-PES for the O_2-HOPG system using existing DFT data from our previous AIMD study.[23] Once the ANN-PES is obtained, it allows us to integrate a large number of trajectories for the different initial alignments probed in the experiments, significantly increasing the statistic of our results and, hence, improving the accuracy of the description of the dynamical properties relevant to the scattering process.

The manuscript is organized as follows. Section 2 describes the methods used to construct and validate the ANN-PES and also, the practical implementation of the ANN-PES dynamics simulations on the present system. The methodology is applied in Section 3 to check the quality of the ANN-PES and to study the alignment effect on the scattering of O_2 from the HOPG surface at

110 and 300 K, where a description, analysis and comparison of our results with the experimental observations by Kurahashi and Kondo is presented. Finally, a summary of the results and the main conclusions of this work are provided in Sec. 4.

2 Computational details

2.1 Neural Network Potential Energy Surface

To obtain the ANN-PES, we used the open source software Atomic Energy Network (aenet)[55] that implements the Neural Network approach developed by Behler and Parrinello.[39] The total energy, E_{tot}, is expressed as the sum of the energy of each atom in the system, E_i, i.e., $E_{tot} = \sum_i E_i$, where the energy of the i-th atom E_i is modeled by a species-dependent Neural Network whose output energy E_i depends on the atom environment.[39] In this work we used the Chebyshev descriptors that were first introduced by Artrith et al[52] and were implemented in the aenet code. These descriptors use two sets of invariant coordinates that separately encode the atomic position and species. The structural descriptor is defined as the expansion coefficients of the radial and angular distribution functions (RDF and ADF, respectively) in a complete basis set ϕ_α:

$$RDF_i(r) = \sum_\alpha c_\alpha^{(2)} \phi_\alpha(r) \quad \text{for } 0 \le r \le r_c \,, \tag{1}$$

$$ADF_i(\theta) = \sum_\alpha c_\alpha^{(3)} \phi_\alpha(\theta) \quad \text{for } 0 \le \theta \le \pi \,. \tag{2}$$

The compositional descriptor is given by the expansion coefficients of the same distribution functions but with atomic contributions that are weighted differently for each chemical species. The chosen basis functions is the first kind Chebyshev polynomials and the expansion coefficients are given by:

$$c_\alpha^{(2)} = \sum_{j \neq i}^{N_{atom}} \phi_\alpha(R_{ij}) f_c(R_{ij}) \omega_{t_j} \,, \tag{3}$$

$$c_{\alpha}^{(3)} = \sum_{j,k\neq i}^{N_{atom}} \phi_{\alpha}(\theta_{ijk}) f_c(R_{ij}) f_c(R_{ik}) \omega_{t_j} \omega_{t_k} \,, \tag{4}$$

where R_{ij} is the distance between a central atom i and its neighbor j and θ_{ijk} is the angle between the vectors $\mathbf{R}_{ij} = \mathbf{R}_j - \mathbf{R}_i$ and $\mathbf{R}_{ik} = \mathbf{R}_k - \mathbf{R}_i$, with $\mathbf{R}_i$ being the position vector of atom i. The cutoff function $f_c(R_{ij}) = 0.5[\cos(R_{ij}\pi/R_c) - 1]$ smoothly decays to zero at the cutoff radius R_c and the weights, ω_{t_j} and ω_{t_k}, are equal to 1 in the structural descriptor and depend on the species in the compositional descriptor. Further details on the derivation of the equations can be found in the work by Artrith et al.[52]

The data set to train, test, and validate the ANN-PES was obtained from our previous AIMD calculations[23] performed with the DFT based Vienna Ab Initio Simulation Package (VASP).[56,57] In those calculations we used the Perdew-Burke-Ernzerhof (PBE)[58] exchange-correlation functional, together with the DFT-D3(BJ) dispersion correction[59,60] in order to account for the van der Waals (vdW) interaction relevant to the O_2-HOPG system. The PBE-D3(BJ) guarantees an adequate description of important system parameters, such as, the HOPG lattice constants ($a = b = 2.47$ Å, $c = 6.70$ Å vs the experimental[61] $a = b = 2.46$ Å, $c = 6.70$ Å), the O_2 binding energy (5.92 eV vs the experimental[62] 5.12 eV), bond length (1.23 Å vs the experimental[62] 1.21 Å) and physisorption energy (0.11 eV vs the experimental[63] 0.10 eV). These calculations performed for a fix initial kinetic energy and incidence angle consisted of 1200 trajectories, 200 for each of the three different initial alignments (see below) and each of the two surface temperatures (110 and 300 K) considered.

The whole data set contains around 2 millions configurations of the O_2-HOPG system with their corresponding DFT energies. Such a huge data set must be carefully sampled in order to reduce the number of structures to introduce in the training data set, while describing correctly the system's configurational space. In our case, the data selection procedure was as follows: First, we randomly chose 100 trajectories of each initial alignment at each surface temperature, reducing to 600 trajectories the initial data set. Second, for each of these selected trajectories, we extract snapshots every 25 fs during the first 300 fs of the dynamics and every 10 fs in the time interval lasting

from 300 fs to the end of the trajectory. This procedure is thus assuring that we do not include in the training set very similar configurations and that we give more importance to the region in which the molecule-surface interaction is stronger. Third, from the resulting set of configurations we selected randomly around 1650 for the different initial alignments at both surface temperatures, resulting in a final data set containing 10 000 configurations. Finally, 12 400 additional configurations were added to the previous data set: 400 are extracted from the O_2 dissociation curves calculated at different distances from the frozen HOPG surface (2.0, 2.5, 3.0, 3.5, 4.0, 5.0, 6.0, 7.0 Å), 9000 from the approximation of O_2 with its molecular axis parallel and perpendicular to a frozen HOPG surface at three different fix internuclear distances (1.18, 1.23, 1.28 Å), and 3000 from calculations in which the first two layers of the HOPG surface are moved along the Z direction, while keeping the X, Y positions of the 36 atoms in the displaced layers fixed. In the end, the resulting training data set contains 22 400 configurations.

For the training procedure, each atom of the system was described by a NN with 16 radial and 12 angular Chebyshev descriptors[55] with cutoff radius R_c = 6.5 Å. We used two hidden layers of 30 nodes each, the hyperbolic tangent with linear twisting as the activation function, and the limited-memory BFGS (Broyden-Fletcher-Goldfarb-Shanno) method[64] as the optimization algorithm. At the beginning of the training process, 10% of the training data set was randomly selected by aenet as test data and the remaining 90% of the original data set as training data. The training process was stopped when the desired convergence of the energy predictions for the training set was reached (RMSE < 0.2 meV/atom) and not over-fitting was observed. A validation of the resulting ANN-PES was carried out by predicting the energies of 20 000 configurations. These configuration were selected from the 600 remaining trajectories that were not used in the training process, using the same methodology explained to build the training set.

2.2 Molecular Dynamics

Molecular dynamics (MD) calculations were performed using the Gas-Surface Reaction Dynamics (GSRD) code. The code was previously developed by some of us to simulate the reaction

dynamics of $CH_{4-x}D_x$ on Pt(111) and Ni(111),[65] CH_4 on Ir(111),[66] and CH_4 on Pt(110) and CO on Cu(110).[67] Here it was extended and adapted to the use of ANN-PESs.

Molecular dynamics on the O_2/HOPG ANN-PES were carried out for incidence conditions corresponding to a (translational) kinetic energy of 0.2 eV with the velocity vector of the O_2 center of mass (CM) defined by a fix polar angle θ_i=22.5° and a random azimuthal angle φ_i that is sampled within the −90° to 90° interval. All trajectories start with a random (x,y) position of the molecule center of mass and located at 7 Å from the surface in order to assure negligible molecule-surface interaction at the beginning of the trajectory. Using these common incidence conditions, two different simulations were performed in which the O_2 zero point energy (ZPE) was or was not initially included.

The first MD simulations study was aimed to validate the ANN-PES. Hence, we used exactly the same initial conditions as in our previous AIMD calculations,[23] that is, the O_2 ZPE was neglected and the initial O_2 internuclear distance was set to the theoretical equilibrium bond length r_e=1.23 Å. Concerning the initial molecular alignment, we should mention that, as we communicated in the erratum[24] to our previous publication, during the preparation of the calculations for the present work we found that the initial molecular alignments denoted as P_X and P_Y and used in our AIMD calculations[23] were not defined as we wrote and as are defined by Kurahashi and Kondo.[15] It is true that, in both cases, the molecular axis was aligned parallel to the graphite surface. However, the molecular alignment named by us P_X and P_Y in our AIMD publication were referred to the graphite directions (zigzag and armchair), and not to the scattering plane. The correct definition is the following. The alignment named P_X in ref. 23 (denoted from here on as P_{ZIG} in the present work) corresponds to the O_2 molecule with its axis parallel to the HOPG surface and initially oriented in the graphite zigzag direction. The alignment named P_Y in ref. 23 (denoted from here on as P_{ARM} in the present work) corresponds to the O_2 molecule with its axis parallel to the HOPG surface and initially oriented in the graphite armchair direction. The definition for P_Z alignment is unchanged and corresponds to the O_2 molecule with the molecular axis perpendicular to the surface. For this validation we integrated 1200 trajectories (200 for each alignment at each surface

temperature) using the same thermalized (110 and 300 K) surface configurations previously used in the AIMD calculations. Each MD trajectory was integrated up to a maximum propagation time of 4 ps with a time step of 0.2 fs.

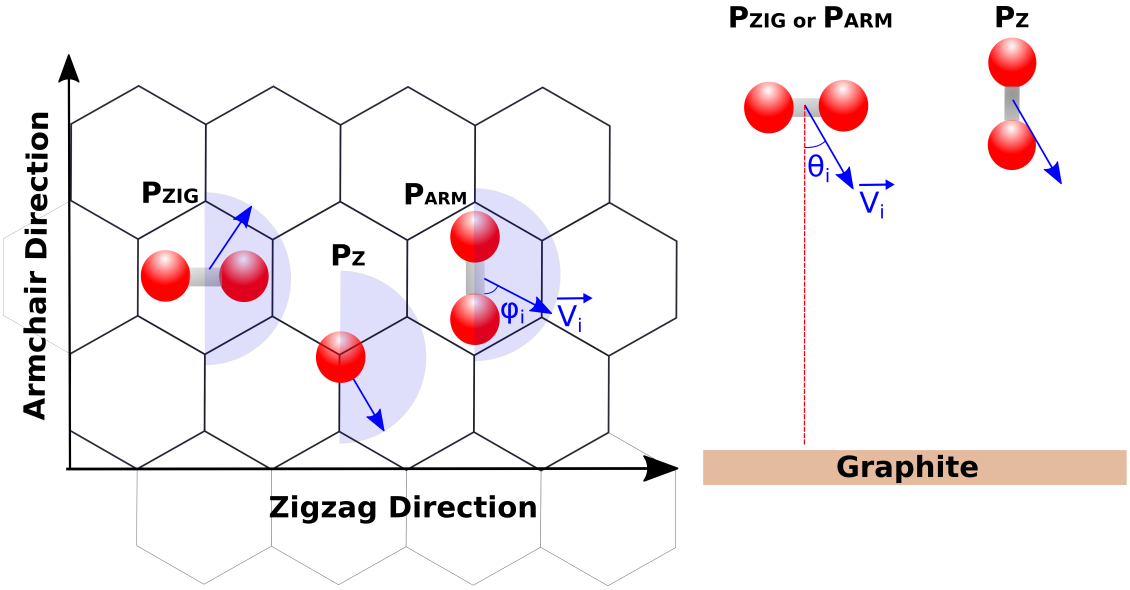

Figure 1: Top (left panel) and side (right panel) views of the initial alignments (P_{ZIG}, P_{ARM}, P_Z) used for the first set of ANN-PES MD simulations of one O_2 molecule impinging over the HOPG surface. The molecular axis is initially oriented parallel to the surface along the zigzag and along the armchair directions for P_X and P_Y, respectively. For P_Z, the molecular axis is initially oriented perpendicular to the surface. The incidence velocity vector of the O_2 center of mass is represented by a blue arrow in each case. Note that the polar incidence angle θ_i is fixed at 22.5° for the three alignments, while the azimuthal incidence angle φ_i is randomly generated within the range marked by the blue shaded areas (left panel).

For the second study, after checking the quality of the ANN-PES, we performed quasi-classical trajectory calculations (QCT) including the O_2 ZPE. Therefore, the initial O_2 internuclear distance and internal momentum were randomly selected for each trajectory according to semi-classical initial conditions corresponding to the (v=0, j=0) ro-vibrational state of the O_2 molecule. In this case, we used the molecular alignments that correspond exactly to those used by Kurahashi and Kondo[15] to rationalize their results, namely P_X, P_Y, and P_Z. These molecular alignments are referred to the scattering plane, which is defined in each trajectory by the surface normal and the velocity vector of O_2 as shown in Figure 2. Specifically, P_X corresponds to the O_2 molecular axis aligned parallel to the surface and perpendicular to the scattering plane, P_Y to the molecular axis

aligned parallel to the surface and within the scattering plane, and P_Z, as in the previous study, to the molecular axis aligned perpendicular to the surface. Under these new incidence conditions 10 000 QCT trajectories per initial O_2 alignment (P_X, P_Y, P_Z) and per surface temperature (110 and 300 K) were carried out using the GSRD MD code. The maximum propagation time was 5 ps with a time step of 0.2 fs.

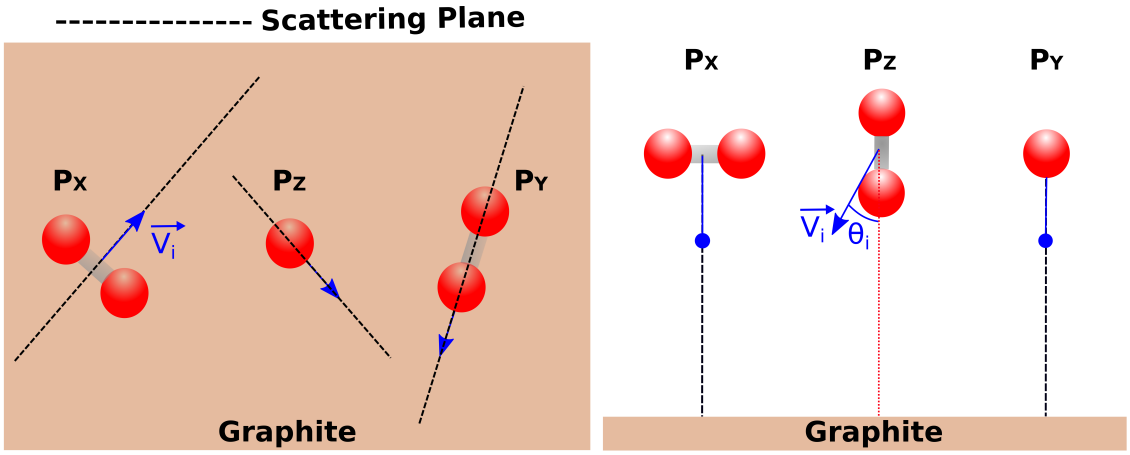

Figure 2: Top (left panel) and side (right panel) views of the initial alignments (P_X, P_Y, P_Z) used for the second set of ANN-PES MD simulations of one O_2 molecule impinging over the HOPG surface. The molecular axis is initially oriented referred to the scattering plane, the graphite direction is undefined because the molecule is initially aligned in function of the initial velocity vector that is random generated in the azimuthal direction (φ_i). For P_Z, the molecular axis is initially oriented perpendicular to the surface. The incidence velocity vector of the O_2 center of mass is represented by a blue arrow in each case. Note that the polar incidence angle θ_i is fixed at 22.5° for the three alignments. In the right hand panel the velocity vectors that end in a point (P_X and P_Y alignments) go out of the plane of the page.

Similarly to the AIMD calculations we performed in ref. 23, the surface temperature was described in this second study with energy-conserving MD simulations by selecting randomly the initial positions and velocities of the moving HOPG surface atoms (those in the two topmost layers) from a canonical set of configurations. For each surface temperature (110 and 300K), the latter was generated by running a canonical trajectory for 20 ps with a time step of 0.2 fs on the ANN-PES. In these canonical trajectories, the HOPG surface is equilibrated to the desired temperature using the Nosé-Hoover thermostat[68,69] implemented in GSRD. Let us remark that this procedure, which is commonly used in gas-surface dynamics simulations,[70–77] is a reasonable approximation

for the usual short simulation times of interest, as shown in ref. 74.

In both sets of simulations, the possible outcomes of the trajectories were either scattering or molecular trapping. The molecule was considered scattered when the distance from the HOPG surface to the O_2 center of mass exceeded 7 Å and the projection on the surface normal (z axis) of the O_2 CM velocity vector points to vacuum. It was considered trapped if after reaching the maximum integration time, the previous condition was not met. The total energy was well conserved in the trajectories with a maximum average error of ~0.2 meV.

Reflected trajectories were discriminated according to the final angle of the center of mass velocity vector with respect to the surface normal (outgoing polar angle (θ_s)) and its deviation with respect to the scattering plane (outgoing azimuthal angle (φ_s)). Molecules for which the deviation φ_s from the scattering plane is equal or smaller than 5° were considered in-plane. Angular distributions of the reflected O_2 were calculated using constant intervals of 2° for both the azimuthal and polar angles. The probability errors were calculated by the usual formula for binomial distributions. The final energy distribution of the reflected molecules was obtained after a standard semi-classical determination of the vibrational, and rotational energies.[78]

3 Results and Discussion

3.1 Atomistic Neural Network Potential Energy Surface Quality

In order to check the accuracy of the obtained ANN-PES, we compare the total energy values that it predicts with those obtained in our previous AIMD calculations for 20 000 configurations (validation set). In Figure 3 we show the correlation obtained between the ANN-PES and AIMD results (left panel) and the histogram of the error distribution (right panel). The good correlation between the ANN-PES and the DFT data is manifested by the fact that all the points on the left hand panel are very close to the perfect correlation line (black line). This is confirmed by the histogram of errors that shows that in the 90% of the tested configurations the absolute value of the error is below 25 meV. It is worth to mention that the total RMSE is 17 meV, which is below the

1% of the variation of the potential energy explored by the system during the dynamics (~ 2 eV).

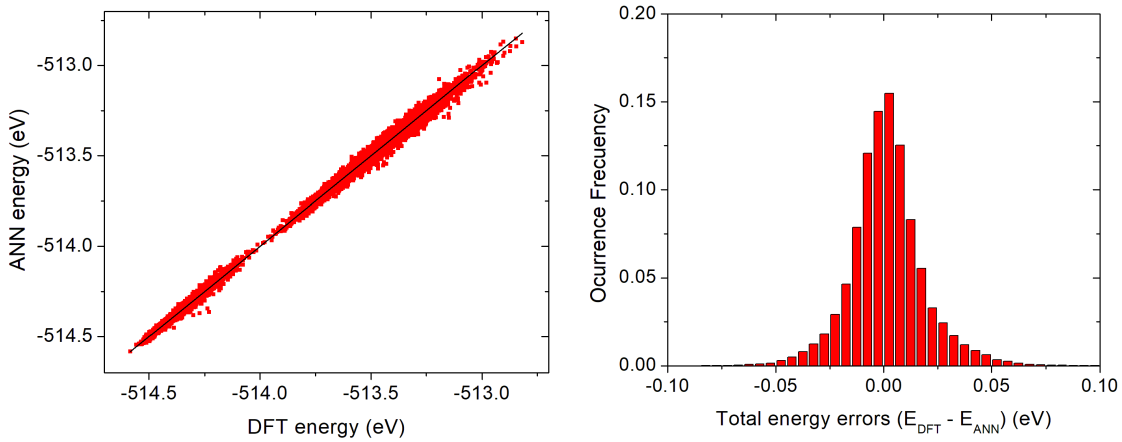

Figure 3: Correlation of the total energy values (left panel) and the distribution of errors (right panel) obtained by the ANN-PES prediction of the DFT validation set. The bin size used in the errors histogram is 0.05 eV.

Although the aenet code does not use the forces in the fitting process, since our aim is to use the ANN-PES to perform molecular dynamics simulations, it is very important to check the accuracy of the ANN-PES to predict the forces. For this reason, we have computed the forces on each atom of the system for the configurations included in our validation set using the ANN-PES and compared them to the DFT data. In Figure 4 we show the correlation diagram for the modulus of the force and the histogram of errors for this quantity for two selected representative atoms: one of the atoms of the O_2 molecule (O1) and one of the C atoms located in the topmost layer of the HOPG surface (C50). Indeed, the figure shows that the ANN-PES is also able to describe the absolute value of the forces. The correlation diagram shows a slightly larger relative dispersion for the absolute value of the forces predicted for the O atom than for the C atom. Still, most of the errors are below 0.5 eV/Å and the obtained total RMSE is below 0.2 eV/Å in both cases.

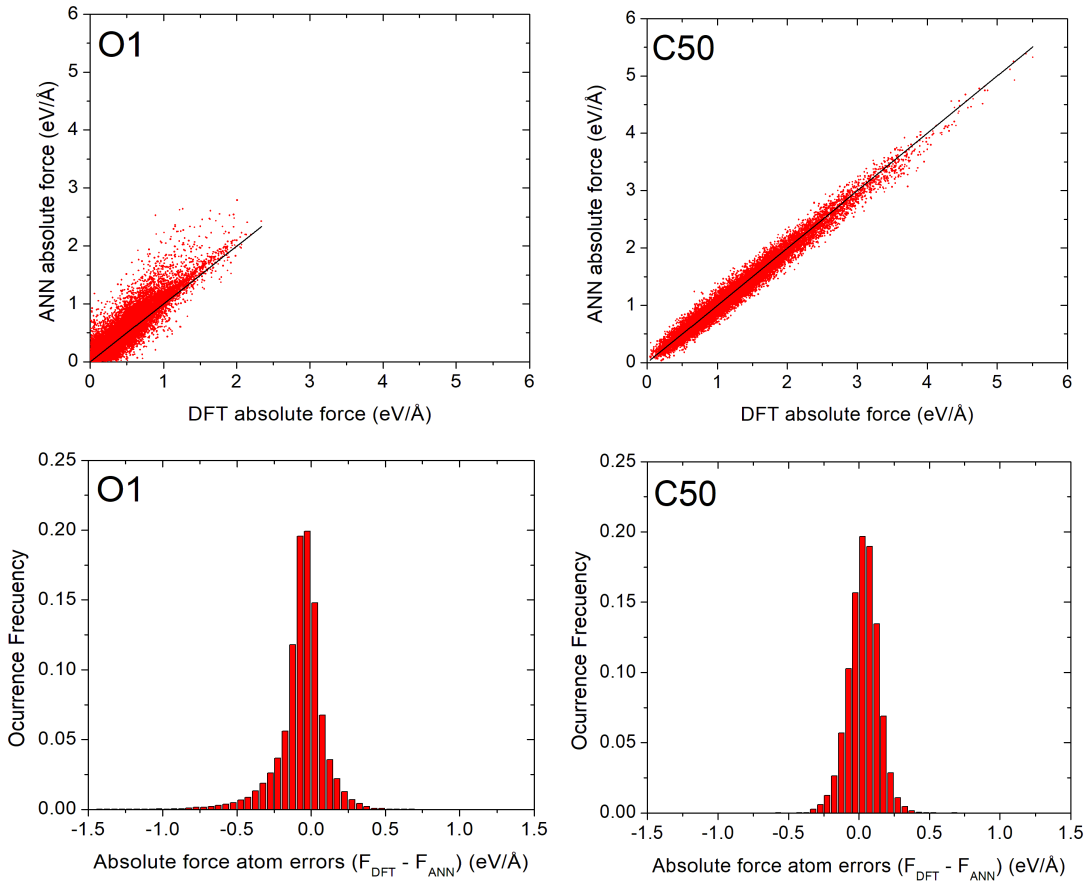

Figure 4: Correlation of the absolute value of the force (top panel) and distribution of errors (bottom panel) obtained by the ANN-PES prediction of the DFT validation set. Left panels show the results for one of the atoms of the O_2 molecule and right panels show the results for one of the C atoms in the topmost layer of the HOPG surface. The bin size used in the errors histogram is 0.05 eV/Å.

Not only the absolute value of the forces but, importantly, also the direction of the forces is well predicted by the ANN-PES. This is shown in Figure 5, in which the distribution of errors for the direction of the forces is shown in terms of the angle between the ANN-PES and the DFT forces, for the two representative atoms of Figure 4. The figure shows that for the O atom the ANN-PES describes correctly the direction of the forces acting on it. In fact, for the 80% of the tested configurations the errors are below 5° respect to DFT reference. The same result is obtained for the other oxygen atom (not shown here). For the C atom the predicted direction is correct too, with 90% of the configurations with errors below 15°. Similar results are obtained also for the rest

of the C atoms present in the system.

In summary, both the absolute value and the direction of the forces are adequately described by the ANN-PES. In particular, this is specially true in the case of the O atoms of the impinging molecule. This constitutes a strong indication of the validity of our ANN-PES to perform accurate molecular dynamics simulations.

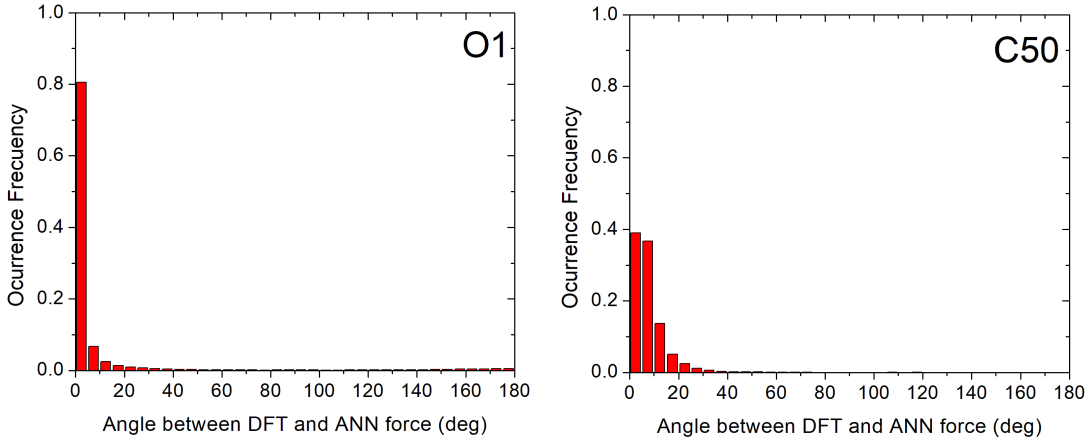

Figure 5: Histogram of the error in the direction of the forces obtained in terms of the difference between the ANN-PES prediction and the DFT results for one of the atoms of the O_2 molecule (left panel) and one of the C atoms in the HOPG topmost layer (right panel). The bin size is 5°.

We have also checked the accuracy of the ANN-PES to reproduce some interesting static features of the O_2-HOPG interaction. In particular, we have analyzed the predictions of the ANN-PES for the O_2 dissociation curves (the dependence of the potential energy on the internuclear distance r at different distances of the O_2 CM from the surface Z_{CM}). Additionally, we have also studied the dependence of the potential energy on Z_{CM} for three different values of r and two different molecular orientations (parallel and perpendicular to the surface). The left panel of Figure 6 shows the comparison between the dependence of the potential energy on r predicted by the ANN-PES (lines) and the one obtained using DFT (symbols) for O_2 parallel to the surface at three different distances from it Z_{CM} = 3, 5 and 7 Å. It is seen that the agreement with the DFT data is almost perfect. The RMSE in the configuration space represented is below 5 meV, which constitutes less than 5% of the O_2 molecule ZPE. This guarantees the correct description of the molecular vibration in our simulations. On the other hand, the right panel shows also the excellent agreement between

the ANN-PES predictions and the DFT results for the potential energy as a function Z_{CM}. The RMSE obtained in this comparison is 2 meV, which is ~2% of the physisorption energy wells for O_2-HOPG obtained in our calculations.

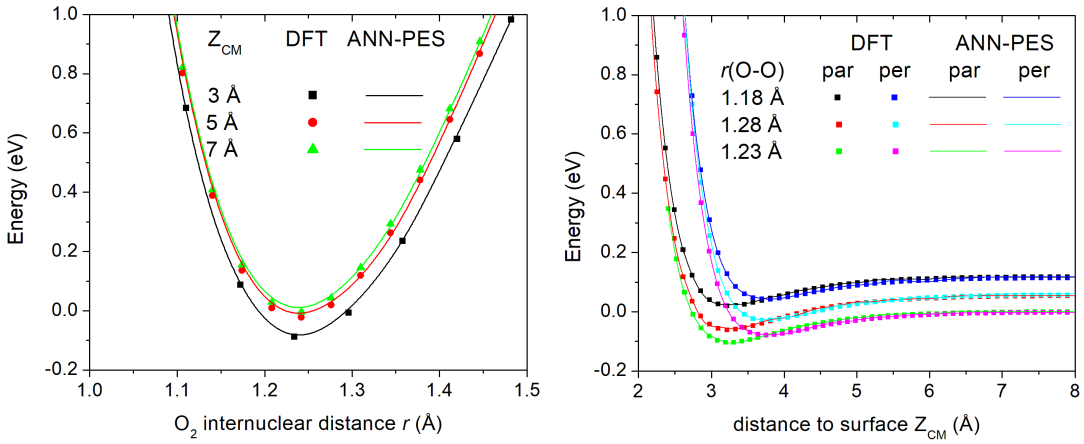

Figure 6: 1D PES for O_2 parallel to the HOPG surface as a function of the interatomic distance r for three different distances from the surface Z_{CM} (left panel). 1D PES for O_2 on HOPG as a function of Z_{CM}, for three different O_2 internuclear distances r and two different molecular orientations, perpendicular and parallel to the surface (right panel). The symbols and lines describe the DFT and the ANN-PES data, respectively.

Finally, as a last validation test for the ANN-PES, we checked its performance in reproducing the outcome of dynamical simulations. To this end, we integrated 1200 MD trajectories (200 for each initial alignment at each surface temperature) with the same initial conditions used in our previous AIMD calculations.[23] The O_2 molecule, without ZPE, was initially set with a kinetic energy of 0.2 eV and velocity vector defined by θ_i=22.5° and φ_i=random. The initial molecular alignments used for these simulations were defined in section 2.2: P_{ZIG} that corresponds to the O_2 molecule with the molecular axis parallel to the HOPG surface and initially oriented in the graphite zigzag direction, P_{ARM} that corresponds to the O_2 molecule with the molecular axis parallel to the HOPG surface and initially oriented in the graphite armchair direction and P_Z that corresponds to the O_2 molecule with the molecular axis perpendicular to the surface.

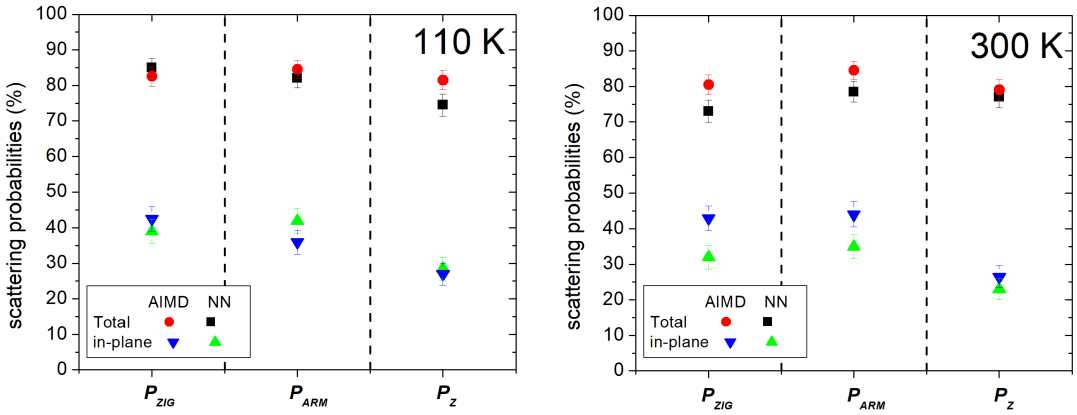

Figure 7: Total and in-plane scattering probabilities (%) for the three molecular initial alignments and the two surface temperatures considered in the ANN-PES and AIMD simulations.

In Figure 7 we compare the total and in-plane scattering probabilities obtained with the ANN-PES simulations and previous AIMD calculations. The results obtained show that the overall agreement between both simulations is good. Only small differences are appreciable for the P_{ZIG} alignment at 300 K, with probabilities obtained by the ANN-PES calculations 10% smaller than the AIMD ones. For the other alignments at both surface temperatures the results can be considered statistically equivalent.

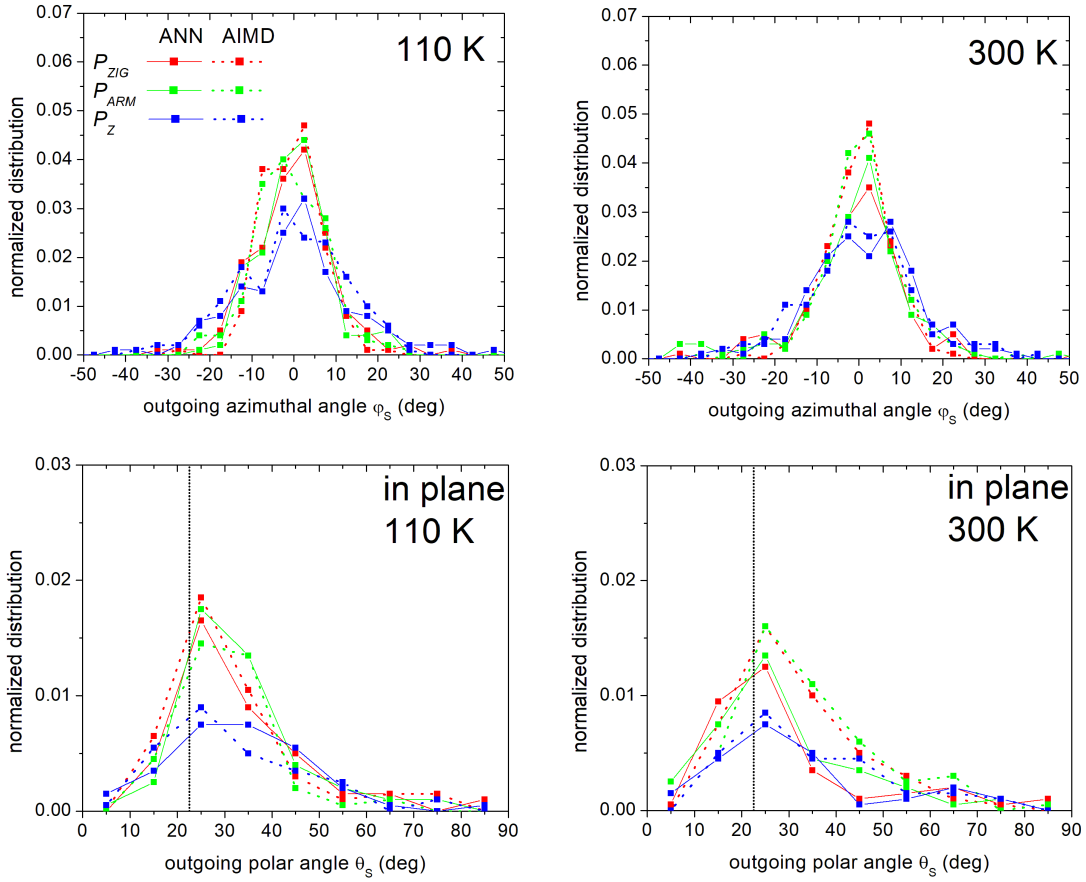

Figure 8: Outgoing azimuthal angle (φ_s) distributions (top panel) measured from the scattering plane of the total reflected O_2 molecules and polar angle (θ_s) distributions (bottom panel) of in-plane reflected O_2 molecules at two surface temperatures (110 and 300 K). The distributions are normalized to the total number of impinging O_2, the bin size is 10°, the symbols are located at the central angle of the bins. The solid lines represent the ANN-PES results and the dot lines the AIMD results. The black dotted line in the polar angle distributions represents the specular angle position (22.5°).

The comparison between ANN-PES (solid lines) and AIMD (dot lines) simulations for the angular distributions at 110 and 300 K represented in Figure 8, also shows that the ANN-PES correctly captures the main features observed in the AIMD simulations. In the case of the outgoing azimuthal angle distributions (top panels), we observe quite the same behavior. First, the peaks of the distributions are located close to 0° (scattering plane), independently of the surface temperature. Second, almost all the side-on aligned molecules are reflected with a maximal azimuthal deviation φ_s of ±20°. Finally, it is clearly seen that the angle distributions for the P_Z alignment

are appreciably wider than for P_X and P_Y. Regarding the polar angle distributions of the in-plane reflected molecules (bottom panels), the same similarity between distributions is observed. In this case, the maximum value is located in the $25 \pm 5°$ bin that contains the specular reflection angle of 22.5°. Additionally, the distributions exhibit an asymmetrical shape around the maximum with a marked preference for angles $\theta_s > \theta_i$.

All in all, the excellent results obtained in the quality check of the ANN-PES and the overall good agreement with the previous AIMD calculations, indicates that the ANN-PES is able to accurately describe the scattering dynamics of O_2 molecules on HOPG surfaces, taking into account all the degrees of freedom present in the system with a much lower computational cost. Also, the possibility of running many more trajectories allows us to achieve a much better statistic.

3.2 Quasi-classical molecular dynamics using ANN-PES

Using the validated ANN-PES, we run 60 000 trajectories (10 000 for each alignment at each surface temperature) under new initial conditions. The O_2 initial kinetic energy is 0.2 eV and the velocity vector is oriented at fixed polar direction defined by θ_i=22.5°. In these new simulations, we take into account the O_2 ZPE, making the simulation more realistic and allowing a better description of the energy transfers that may occur during the collision with the HOPG surface. Also, for these simulations, the initial O_2 alignments is set to reproduce exactly the alignments used by Kurahashi and Kondo[15] to rationalize their experimental results[15] namely P_X, P_Y, P_Z, which are referred, as described in section 2.2, to the scattering plane as follows: P_X corresponds to the molecular axis aligned parallel to the surface and perpendicular to the scattering plane, P_Y to the molecular axis aligned parallel to the surface and inside the scattering plane, and P_Z to the molecular axis aligned perpendicular to the surface.

3.3 Scattering probabilities and angular distributions

Table 1 summarizes the total and in-plane scattering probabilities obtained from our ANN-PES MD simulations for each incidence alignment and surface temperature. Total probabilities are

calculated considering all the reflected trajectories (i.e., irrespective of the outgoing polar (θ_s) and azimuthal (φ_s) angles), while in-plane probabilities refer to molecules reflected with an azimuthal deviation from the scattering plane $|\varphi_s| \leq 5°$. The results show that the total scattering probability is almost independent of the initial alignment of the molecule and surface temperature. In all cases, approximately out 9 of 10 molecules are reflected, most of them after a single binary collision with the HOPG surface. These results point out that the scattering of O_2 from HOPG can be viewed as a rather direct process and are in perfect agreement with previous theoretical and experimental reports[2,3,13–15,23] about the system .

Table 1: Total and in-plane scattering probabilities (%) for the three molecular initial alignments and two surface temperatures considered in the ANN-PES MD simulations. The percentage of trajectories that are reflected after one single collision with the surface is within parenthesis.

T(K)		P_X	P_Y	P_Z
110	total	85.8±0.5 (60.9)	85.7±0.4 (60.6)	86.3±0.3 (58.6)
	in-plane	42.5±0.5 (36.7)	26.2±0.4 (21.2)	30.4±0.5 (23.3)
300	total	89.9±0.3 (68.5)	89.8±0.3 (67.9)	91.3±0.3 (63.9)
	in-plane	47.0±0.5 (41.1)	29.4±0.5 (24.5)	34.6±0.5 (26.9)

Table 1 shows that there exist differences for the in-plane scattering probabilities between molecules with different alignments. Specifically, the probability of detecting in-plane scattered molecules coming from P_X alignment is ∼(1.3-1.6) times greater than from the other cases (P_Y, P_Z). The results indicate that when the O_2 molecular axis is initially contained in the scattering plane, which is the case for P_Y and P_Z, the molecules are more likely to be reflected out of the scattering plane. The major proportion of out-of-plane molecules obtained in our simulations for these two alignments was previously observed by Kurahashi and Kondo.[15] They rationalized this effect by the fact that molecules with its axis in the scattering plane are more sensitive to the corrugation of the surface perpendicular to the scattering plane, which is the property that generates out-of-plane scattering.

Also, the fact that the total number of reflected molecules hardly depends on their initial alignment means that the alignment dependence of the in-plane probabilities is not caused by an increase

in the number of trapped molecules. The reason must be related to a more efficient deviation from the scattering plane of the P_Y- and P_Z-aligned molecules.

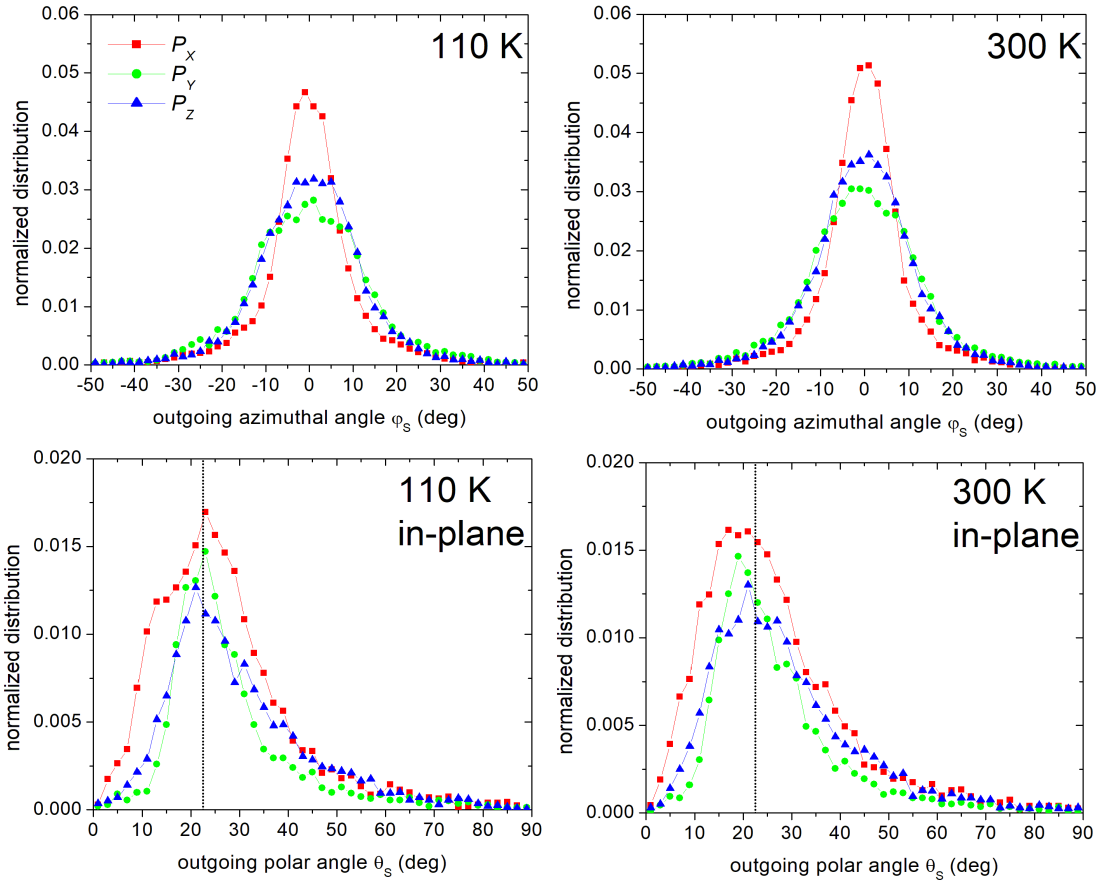

Figure 9: Outgoing azimuthal angle (φ_s) distributions (top panel) of the reflected O_2 molecules and polar angle (θ_s) distributions (bottom panel) of in-plane reflected O_2 molecules at two surface temperatures (110 and 300 K). The dotted line in the polar angle distributions represents the specular angle position (22.5°). The distributions are normalized to the total number of impinging O_2, the bin size is 2°, the symbols are located at the central angle of the bins.

The outgoing azimuthal angle distributions plotted in the top panels of Figure 9 for the reflected O_2 confirm that this is actually the case. The distributions for P_Y and P_Z alignment are wider, particularly in $-20° \leq \varphi_s \leq 20°$ interval, while in the in-plane range defined as $-5° \leq \varphi_s \leq 5°$ clear differences exist between P_X and the other alignments. The peak intensities for the angular distributions, at both surface temperatures, are ~1.5 higher for P_X than for P_Y and P_Z alignments. Also, independently of the surface temperature, almost all the molecules are reflected with a maximal azimuthal deviation φ_s of ±30°.

In the case of the polar angle distributions of the in-plane reflected molecules (bottom panel), for all the studied alignments the distribution peaks are located very close to the specular angle 22.5° (dotted line). The P_X distributions at both surface temperatures are appreciably wider and higher than the P_Y and P_Z ones. Furthermore, the distributions extend up to large outgoing angles of $70° - 80°$ and exhibit an asymmetrical shape around the maximum with a marked preference for angles $\theta_s > \theta_i$. This behavior suggests that there is larger energy loss in the perpendicular than in the parallel degree of freedom as we previously observed in AIMD calculations using slightly different molecular alignments. The increase in the number of trajectories that can be calculated using the ANN-PES respect to the AIMD simulations, allows us to obtain statistically meaningful information on some dynamical aspects that cannot be captured in the latter simulations due to the poorer achievable statistics. In particular, this is the case of the alignment dependence of the in-plane scattering probabilities at the specular scattering angle, which can be compared to the experimental observations. Certainly, as shown in Figure 9, the heights of the P_X, P_Y, and P_Z in-plane distributions at the specular angle decrease following this order at both surface temperatures. At 110 K (300 K) surface temperature, the values of the scattering probabilities at the specular angle are 0.017 (0.016), 0.015 (0.012), and 0.011 (0.011) for the P_X, P_Y, and P_Z alignments, respectively.

To compare the obtained in-plane polar angular distributions with the experiments by Kurahashi and Kondo[15] it is necessary to take into account some considerations. In the experimental incidence conditions the ranges of initial translational energy and incidence polar angle (measured from surface normal) were $0.08 - 0.25$ eV and $\theta_i = 0° - 45°$, respectively. The azimuthal direction of the molecular beam was chosen randomly. The experimental set-up only detects molecules scattered in the scattering plane (acceptance angle of 1.5°) and reflected with angles θ_s such that $\theta_i + \theta_s = 45°$. Thus, the reported angular distributions as a function of θ_s were obtained varying θ_i.

For these ANN-PES calculations we used a single angle of incidence ($\theta_i = 22.5°$) and the azimuthal direction was varied randomly in the different simulations. Also, a bigger acceptance angle (5°) to define the in-plane scattering detection was used and we were able to detect all the scattered

molecules (out and in-plane). The use of a bigger acceptance angle with respect to the experiments is related to statistical reasons. The number of trajectories integrated in the present simulations significantly improves the statistics obtained in our previous AIMD calculations but it is still insufficient to allow us to use a smaller acceptance angle. When we tested an acceptance angle of 1.5° we obtained in-plane scattering probabilities ~ 3 times lower for all the alignments, which considerably limited the statistics of the results. Note, that with the incidence conditions chosen by us the experimental detection condition ($\theta_i + \theta_s = 45°$) is fulfilled at the specular direction $\theta_s = 22.5°$ which is highlighted in Figure 9 with a dot line. At this detection angle, our results for the alignment dependence of the scattering probabilities (see above) are in qualitative agreement with the experimental values obtained by Kurahashi and Kondo (Figure 3 in ref. 15) at a similar incidence energy (0.18 eV). As in our case, the values of the experimental scattering probabilities, from the higher value to the lower one, follow the order P_X, P_Y, P_Z. Moreover, they find that the scattering probability for the P_Z alignment is noticeably smaller than that of P_X, whereas the one for P_Y is only slightly smaller.

In addition, in our simulation we reproduce a very interesting feature observed by Kurahashi and Kondo[15] concerning the shape of the P_Y angular distributions. The full width at half maximum that we observe for these distributions are, as in the experiments, narrower than the distributions for the other two alignments. The reason for this particular behavior should be related, as was previously suggested by Kurahashi and Kondo,[15] with the corrugation felt by the O_2 molecule inside the scattering plane. It is expected that P_Y molecules feel a smaller corrugation within the scattering plane which explains their calculated and measured narrower θ-angle distributions.

3.4 Energy transfer and rotational distributions

Figure 10 shows how the final energy of the in-plane reflected molecules is distributed between the internal and translational degrees of freedom (DOF). For these simulations, where the ZPE was considered in the initial conditions we are able to separate the components of the internal energy in vibrational and rotational modes.

The results at 110 and 300 K are similar with small differences of around 30 meV respect to the final average translational energies of the molecules and the energy exchange with the surface. Our simulations show that at 110 K around 20% of the translational energy is transferred to the surface. At 300 K the transfer occurs mainly between translational and rotational modes and in average no energy is delivered to or received by the surface.

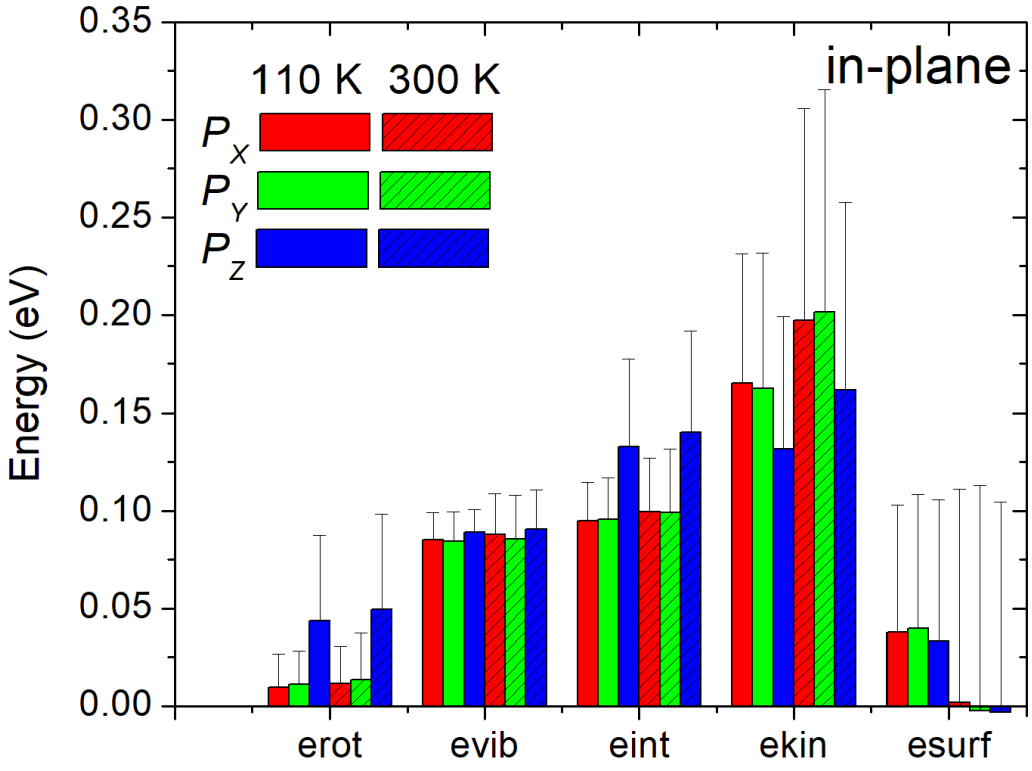

Figure 10: Partition of the final energy of the in-plane scattered O_2 molecules into rotational (erot), vibrational (evib), total internal (eint) and translational energy (ekin), and the energy transferred to the surface (esurf).

Regarding the dependence on the initial alignment, the main differences appear when comparing the rotational energy values of P_Z with P_X and P_Y in-plane scattered molecules. The final rotational energy for head-on molecules is 5 times greater than for the side-on ones. In contrast, the final vibrational energy is almost the same for all the alignments. It remains unchanged respect to its initial value, corresponding to the energy value of the vibrational ground state (v=0) of the O_2 molecule. Also, we observe that the molecules with perpendicular orientations are more likely to

lose translational energy. For the present calculations we estimate an average translational energy lost of $\sim 30\%$ for the P_Z alignment and $\sim 10\%$ for the P_X and P_Y ones. In addition, the translational energy loss is enhanced at lower surface temperature.

Taking into account that all the in-plane molecules detected, independent of their initial alignments, keep their initial vibrational state unaltered, it is possible to summarize that for head-on molecules the energy transfer occurs mainly from translational to rotational modes upon collision with the surface. In contrast, the side-on molecules are weakly rotational excited. Additionally, the results seem to indicate that side-on molecules transfer energy more efficiently to the surface. The present results are consistent with the dependence of the energy transfer on the stereodynamics reported by Rutigliano and Pirani[14] and by some of us using AIMD[23] for the studied system.

For further details we present in Figure 11 the rotational distributions of in-plane scattered molecules obtained for the two surface temperatures considered. The distributions corresponding to parallel orientations (P_X and P_Y) are very similar, showing two peaks located at j=1 and j=7 rotational states and decaying very fast towards higher rotational levels (j=17). The first peak (j=1) corresponds to scattered molecules that keep their initial vibrational and rotational state almost unaltered, being barely influenced by the interaction with the surface and experimenting rather elastic collision. This molecules represent around 15% and 12% of detected O_2 at 110 and 300 K respectively. Interestingly, slight differences, mainly at 110 K (~4%), can be observed between P_X and P_Y distributions, pointing out that the microscopic interaction mechanism could be very sensitive to the initial molecule alignment. The second peak (j=7), corresponds to the most probable rotational level that can be populated given the average available internal energy of the molecules detected in our simulations and is a clear signature of inelastic collisions with the surface. Also, when representing only the rotational distribution for the side-on scattered molecules that experiment more that one collision with the surface (not shown here), we obtain a bell shaped rotational distribution with a single peak at j=7.

On the other hand, the P_Z distributions show almost equally populated rotational levels up to a high excited rotational state (j=35). The shape of the distributions clearly indicate that a very

efficient rotational energy redistribution takes place after the interaction of the P_Z molecules with the surface and that rotational excitation is a fingerprint of head-on collisions.

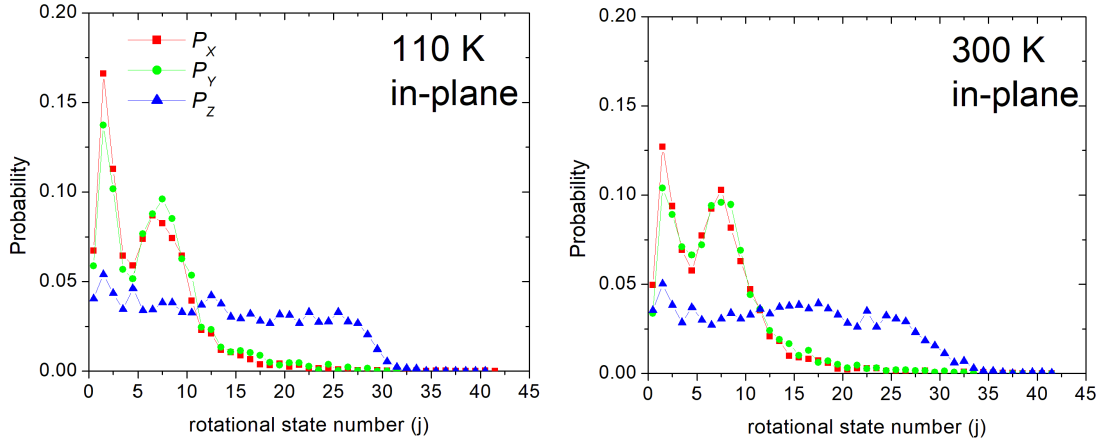

Figure 11: Rotational distribution of the in-plane scattered O_2 molecules. The distributions are normalized to the total number of in-plane reflected O_2, the bin size is 1.

4 Conclusions

In summary, we have obtained a High Dimensional Atomistic Neural Network Potential Energy Surface capable of describing accurately the O_2-HOPG interaction for all the relevant degrees of freedom of the system. This allows us to perform molecular dynamics studies at a much lower computational cost than AIMD calculations. The ANN-PES has been validated comparing its predictions with a large DFT reference data set and performing a molecular dynamics study. The results showed low errors for the energy and forces predicted by the ANN-PES, as well as, an overall agreement with our previous AIMD study. The current ANN-PES inside the GSRD-code is $\sim$ 700 time faster computing a single point (energy and force) than our previous AIMD calculations.

Using the validated ANN-PES, we have performed a molecular dynamics study of the alignment resolved O_2 scattering from HOPG with initial conditions that reproduce the alignments used by Kurahashi and Kondo[15] to explain their experimental results. Scattering probabilities, angu-

lar distributions, energy transfers, and rotational distributions at two surface temperatures (110 and 300 K) of aligned molecules (P_X, P_Y and P_Z) with an incidence energy of 0.2 eV have been computed.

Our new results confirm that the trapping on this system is rather minor and that depends very weakly on surface temperature and initial alignment of the molecules. Roughly, 10% of the molecules remain trapped after the 5 ps simulation time and also most of the reflected molecules are scattered after a single collision. Regarding the in-plane scattered molecules, we found that the probability of detecting molecules coming from P_X alignment is greater than for P_Y and P_Z ones. Also, at the specular outgoing direction ($\theta_s = 22.5°$), we observed clear differences between the intensity for the angular distributions corresponding to P_X and P_Z alignments, while, an incipient intensity order ($P(P_X) > P(P_Y) > P(P_Z)$) appears, in qualitative agreement with the experimental observations.[15]

We have also performed an analysis of the alignment dependence of the final energy of the in-plane scattered molecules and its distribution among the different degrees of freedom. The results can be summarized as follows: (i) The transfer of energy to the surface is almost independent of the initial alignment at 110 K and is negligible at 300 K, (ii) the rotational excitation upon collision with the surface is much more favorable for P_Z molecules than for P_X and P_Y molecules,(iii) the scattered molecules keep their initial vibrational state, (iv) the final outcome is that $\sim$ 20 % more of translational energy is lost in the case of end-on molecules as compared to side-on molecules.

All in all, the use of the ANN-PES allowed us to run a huge number of trajectories (10 000 for each alignment at two different surface temperatures) improving the statistical accuracy of our calculations. The obtained results are in good agreement with the experimental results of Kurahashi and Kondo[15] reproducing the shape of the angular distributions and the alignment dependence observed in the experiments. They also provide important information about the underlying physics involved in the scattering process and answer open questions from the experiments, (i) the alignment dependence of the in-plane probabilities is not caused by an increase in the number of trapped molecules but by the increase of the direct out-of-plane scattering depending on the initial molecule

orientation, (ii) the lower final translational energy of head-on molecules is not due to an increased energy lost to the surface but to a more efficient energy transfer from the translational to the rotational degrees of freedom. The present ANN-PES is able to accurately reproduce the scattering process of O_2 on HOPG surfaces, at lower computational cost, and can be used to perform simulations for multiple initial conditions, such as, changing the incidence conditions and detection geometry, molecule impinges along specific directions of the benzene ring, among others.

5 Acknowledgments

We acknowledge financial support by the Gobierno Vasco-UPV/EHU project IT1246-19, and the Spanish Ministerio de Ciencia e Innovación [Grant No. PID2019-107396GB-I00/AEI/10.13039/501100011033], as well as Agencia Nacional de Promoción de la Investigación, el Desarrollo Tecnológico y la Innovación (project PICT-2016 2750). This research was conducted in the scope of the Transnational Common Laboratory (LTC) "QuantumChemPhys – Theoretical Chemistry and Physics at the Quantum Scale". Computational resources were provided by the DIPC computing center.

References

(1) McKee, D.; McCarroll, B. The reactivity of graphite surfaces with atoms and molecules of hydrogen, oxygen and nitrogen. *Carbon* **1972**, *10*, 328.

(2) Oh, J.; Kondo, T.; Arakawa, K.; Saito, Y.; Hayes, W. W.; Manson, J. R.; Nakamura, J. Angular intensity distribution of a molecular oxygen beam scattered from a graphite surface. *J. Phys. Chem. A* **2011**, *115*, 7089–7095.

(3) Hayes, W. W.; Oh, J.; Kondo, T.; Arakawa, K.; Saito, Y.; Nakamura, J.; Manson, J. R. Scattering of O_2 from a graphite surface. *J. Phys.: Condens. Matter* **2012**, *24*, 104010.

(4) Murray, V. J.; Marshall, B. C.; Woodburn, P. J.; Minton, T. K. Inelastic and reactive scattering

dynamics of hyperthermal O and O_2 on hot vitreous carbon surfaces. *J. Phys. Chem. C* **2015**, *119*, 14780–14796.

(5) Bagsican, F. R.; Winchester, A.; Ghosh, S.; Zhang, X.; Ma, L.; Wang, M.; Murakami, H.; Talapatra, S.; Vajtai, R.; Ajayan, P. M. et al. Adsorption energy of oxygen molecules on graphene and two-dimensional tungsten disulfide. *Sci. Rep.* **2017**, *7*.

(6) Dubský, J.; Beran, S. Quantum chemical study of oxygen adsorption on graphite. *Surf. Sci.* **1979**, *79*, 53–62.

(7) Lamoen, D.; Persson, B. N. J. Adsorption of potassium and oxygen on graphite: A theoretical study. *J. Chem. Phys.* **1998**, *108*, 3332–3341.

(8) Incze, A.; Pasturel, A.; Chatillon, C. Oxidation of graphite by atomic oxygen: a first-principles approach. *Surf. Sci.* **2003**, *537*, 55–63.

(9) Giannozzi, P.; Car, R.; Scoles, G. Oxygen adsorption on graphite and nanotubes. *J. Chem. Phys.* **2003**, *118*, 1003–1006.

(10) Paci, J. T.; Upadhyaya, H. P.; Zhang, J.; Schatz, G. C.; Minton, T. K. Theoretical and experimental studies of the reactions between hyperthermal $O(^3P)$ and graphite: Graphene-Based direct dynamics and beam-surface scattering approaches. *J. Phys. Chem. A* **2009**, *113*, 4677–4685.

(11) Morón, V.; Gamallo, P.; Sayós, R. DFT and kinetics study of O/O_2 mixtures reacting over a graphite (0001) basal surface. *Theor. Chem. Acc.* **2011**, *128*, 683–694.

(12) Morón, V.; Martin-Gondre, L.; Gamallo, P.; Sayós, R. Dynamics of the oxygen molecules scattered from the graphite (0001) surface and comparison with experimental data. *J. Phys. Chem. C* **2012**, *116*, 21482–21488.

(13) Majumder, M.; Gibson, K. D.; Sibener, S. J.; Hase, W. L. Chemical dynamics simulations and

scattering experiments for O_2 collisions with graphite. *J. Phys. Chem. C* **2018**, *122*, 16048–16059.

(14) Rutigliano, M.; Pirani, F. On the influence of rotational motion of oxygen molecules on the scattering from graphite surfaces. *J. Phys. Chem. C* **2019**, *123*, 11752–11762.

(15) Kurahashi, M.; Kondo, T. Alignment-resolved O_2 scattering from highly oriented pyrolytic graphite and LiF(001) surfaces. *Phys. Rev. B* **2019**, *99*, 045439.

(16) Vattuone, L.; Savio, L.; Pirani, F.; Cappelletti, D.; Okada, M.; Rocca, M. Interaction of rotationally aligned and of oriented molecules in gas phase and at surfaces. *Prog. Surf. Sci.* **2010**, *85*, 92–160.

(17) Kurahashi, M.; Yamauchi, Y. Steric effect in O_2 sticking on Al(111): Preference for parallel geometry. *Phys. Rev. Lett.* **2013**, *110*.

(18) Kurahashi, M. Oxygen adsorption on surfaces studied by a spin- and alignment-controlled O_2 beam. *Prog. Surf. Sci.* **2016**, *91*, 29–55.

(19) Godsi, O.; Corem, G.; Alkoby, Y.; Cantin, J. T.; Krems, R. V.; Somers, M. F.; Meyer, J.; Kroes, G.-J.; Maniv, T.; Alexandrowicz, G. A general method for controlling and resolving rotational orientation of molecules in molecule-surface collisions. *Nat. Commun.* **2017**, *8*, 15357.

(20) Kurahashi, M. Chemisorption of aligned O_2 on Ag(110). *J. Chem. Phys.* **2019**, *151*, 084702.

(21) Cao, K.; van Lent, R.; Kleyn, A. W.; Kurahashi, M.; Juurlink, L. B. F. Steps on Pt stereodynamically filter sticking of O_2. *Proc. Natl. Acad. Sci. U.S.A.* **2019**, *116*, 13862–13866.

(22) Alkoby, Y.; Chadwick, H.; Godsi, O.; Labiad, H.; Bergin, M.; Cantin, J. T.; Litvin, I.; Maniv, T.; Alexandrowicz, G. Setting benchmarks for modelling gas-surface interactions using coherent control of rotational orientation states. *Nat. Commun* **2020**, *11*.

(23) Rivero Santamaría, A.; Alducin, M.; Diez Muiño, R.; Juaristi, J. I. Ab Initio Molecular Dynamics Study of Alignment Resolved O_2 Scattering from Highly Oriented Pyrolytic Graphite. *J. Phys. Chem. C* **2019**, *123*, 31094–31102.

(24) Rivero Santamaría, A.; Alducin, M.; Díez Muiño, R.; Juaristi, J. I. Correction to "Ab Initio Molecular Dynamics Study of Alignment Resolved O2 Scattering from Highly Oriented Pyrolytic Graphite". *J. Phys. Chem. C* **2021**, *125*, 1170–1170.

(25) Busnengo, H. F.; Crespos, C.; Dong, W.; Rayez, J. C.; Salin, A. Classical dynamics of dissociative adsorption for a nonactivated system: The role of zero point energy. *J. Chem. Phys.* **2002**, *116*, 9005–9013.

(26) Lozano, A.; Gross, A.; Busnengo, H. F. Adsorption dynamics of H_2 on Pd(100) from first principles. *Phys. Chem. Chem. Phys.* **2009**, *11*, 5814.

(27) Díaz, C.; Pijper, E.; Olsen, R. A.; Busnengo, H. F.; Auerbach, D. J.; Kroes, G. J. Chemically Accurate Simulation of a Prototypical Surface Reaction: H_2 Dissociation on Cu(111). *Science* **2009**, *326*, 832–834.

(28) Ramos, M.; Minniti, M.; Díaz, C.; Farías, D.; Miranda, R.; Martín, F.; Martínez, A. E.; Busnengo, H. F. Environment-driven reactivity of H_2 on PdRu surface alloys. *Phys. Chem. Chem. Phys.* **2013**, *15*, 14936.

(29) Goikoetxea, I.; Juaristi, J. I.; Díez Muiño, R.; Alducin, M. Surface Strain Improves Molecular Adsorption but Hampers Dissociation for N_2 on the Fe/W(110) Surface. *Phys. Rev. Lett.* **2014**, *113*, 066103.

(30) Goikoetxea, I.; Meyer, J.; Juaristi, J. I.; Alducin, M.; Reuter, K. Role of Physisorption States in Molecular Scattering: A Semilocal Density-Functional Theory Study on O_2/Ag(111). *Phys. Rev. Lett.* **2014**, *112*, 156101.

(31) Lončarić, I.; Alducin, M.; Juaristi, J. I. Dissociative dynamics of O_2 on Ag(110). *Phys. Chem. Chem. Phys.* **2015**, *17*, 9436–9445.

(32) Jiang, B.; Guo, H. Dynamics of Water Dissociative Chemisorption on Ni(111): Effects of Impact Sites and Incident Angles. *Phys. Rev. Lett.* **2015**, *114*, 166101.

(33) Nihill, K. J.; Hund, Z. M.; Muzas, A.; Díaz, C.; del Cueto, M.; Frankcombe, T.; Plymale, N. T.; Lewis, N. S.; Martín, F.; Sibener, S. J. Experimental and theoretical study of rotationally inelastic diffraction of $H_2(D_2)$ from methyl-terminated Si(111). *J. Chem. Phys.* **2016**, *145*, 084705.

(34) Lončarić, I.; Alducin, M.; Juaristi, J. I. Molecular dynamics simulation of O_2 adsorption on Ag(110) from first principles electronic structure calculations. *Phys. Chem. Chem. Phys.* **2016**, *18*, 27366–27376.

(35) Muzas, A. S.; del Cueto, M.; Gatti, F.; Somers, M. F.; Kroes, G. J.; Martín, F.; Díaz, C. H_2/LiF(001) diffractive scattering under fast grazing incidence using a DFT-based potential energy surface. *Phys. Rev. B* **2017**, *96*, 205432.

(36) Nosir, M. A.; Martin-Gondre, L.; Bocan, G. A.; Díez Muiño, R. Dissociative adsorption dynamics of nitrogen on a Fe(111) surface. *Phys. Chem. Chem. Phys.* **2017**, *19*, 24626–24635.

(37) Ramos, M.; Díaz, C.; Martínez, A. E.; Martín, F.; Busnengo, H. F. Thickness-Dependent Reactivity of O_2 on Cu Layers Grown on Ru(0001) Surfaces. *J. Phys. Chem. C* **2018**, *122*, 15529–15538.

(38) Zhou, Y.; Zhou, L.; Hu, X.; Xie, D. Dynamics Studies of O_2 Collision on Pt(111) Using a Global Potential Energy Surface. *J. Phys. Chem. C* **2020**, *124*, 10573–10583.

(39) Behler, J.; Parrinello, M. Generalized neural-network representation of high-dimensional potential-energy surfaces. *Phys. Rev. Lett.* **2007**, *98*, 146401.

(40) Kolb, B.; Luo, X.; Zhou, X.; Jiang, B.; Guo, H. High-Dimensional Atomistic Neural Network Potentials for Molecule-Surface Interactions: HCl Scattering from Au(111). *J. Phys. Chem. Lett.* **2017**, *8*, 666–672.

(41) Shakouri, K.; Behler, J.; Meyer, J.; Kroes, G.-J. Accurate Neural Network Description of Surface Phonons in Reactive Gas-Surface Dynamics: N_2 + Ru(0001). *J. Phys. Chem. Lett.* **2017**, *8*, 2131–2136.

(42) Liu, Q.; Zhou, X.; Zhou, L.; Zhang, Y.; Luo, X.; Guo, H.; Jiang, B. Constructing High-Dimensional Neural Network Potential Energy Surfaces for Ga-Surface Scattering and Reactions. *J. Phys. Chem. C* **2018**, *122*, 1761–1769.

(43) Zhang, Y.; Zhou, X.; Jiang, B. Bridging the Gap between Direct Dynamics and Globally Accurate Reactive Potential Energy Surfaces Using Neural Networks. *J. Phys. Chem. Lett.* **2019**, *10*, 1185–1191.

(44) Huang, M.; Zhou, X.; Zhang, Y.; Zhou, L.; Alducin, M.; Jiang, B.; Guo, H. Adiabatic and nonadiabatic energy dissipation during scattering of vibrationally excited CO from Au(111). *Phys. Rev. B* **2019**, *100*, 201407.

(45) del Cueto, M.; Zhou, X.; Zhou, L.; Zhang, Y.; Jiang, B.; Guo, H. New Perspectives on CO_2 - Pt(111) Interaction with a High-Dimensional Neural Network Potential Energy Surface. *J. Phys. Chem. C* **2020**, *124*, 5174–5181.

(46) Hu, C.; Zhang, Y.; Jiang, B. Dynamics of H_2O Adsorption on Pt(110)-(1 x 2) Based on a Neural Network Potential Energy Surface. *J. Phys. Chem. C* **2020**, *124*, 23190–23199.

(47) Jiang, B.; Li, J.; Guo, H. High-Fidelity Potential Energy Surfaces for Gas-Phase and Gas-Surface Scattering Processes from Machine Learning. *J. Phys. Chem. Lett.* **2020**, *11*, 5120–5131.

(48) Behler, J. Atom-centered symmetry functions for constructing high-dimensional neural network potentials. *J. Chem. Phys.* **2011**, *134*, 074106.

(49) Behler, J. Constructing high-dimensional neural network potentials: A tutorial review. *Int. J. Quantum Chem.* **2015**, *115*, 1032–1050.

(50) Behler, J. First Principles Neural Network Potentials for Reactive Simulations of Large Molecular and Condensed Systems. *Angew. Chem.* **2017**, *56*, 12828–12840.

(51) Bartók, A. P.; Kondor, R.; Csányi, G. On representing chemical environments. *Phys. Rev. B* **2013**, *87*.

(52) Artrith, N.; Urban, A.; Ceder, G. Efficient and accurate machine-learning interpolation of atomic energies in compositions with many species. *Phys. Rev. B* **2017**, *96*, 014112.

(53) Imbalzano, G.; Anelli, A.; Giofré, D.; Klees, S.; Behler, J.; Ceriotti, M. Automatic selection of atomic fingerprints and reference configurations for machine-learning potentials. *J. Chem. Phys.* **2018**, *148*, 241730.

(54) Li, J.; Song, K.; Behler, J. A critical comparison of neural network potentials for molecular reaction dynamics with exact permutation symmetry. *Phys. Chem. Chem. Phys.* **2019**, *21*, 9672–9682.

(55) Artrith, N.; Urban, A. An implementation of artificial neural-network potentials for atomistic materials simulations: Performance for TiO2. *Comput. Mater. Sci* **2016**, *114*, 135–150.

(56) Kresse, G.; Furthmüller, J. Efficiency of ab-initio total energy calculations for metals and semiconductors using a plane-wave basis set. *Comput. Mater. Sci.* **1996**, *6*, 15–50.

(57) Kresse, G.; Furthmüller, J. Efficient iterative schemes for ab-initio total-energy calculations using a plane-wave basis set. *Phys. Rev. B* **1996**, *54*, 11169–11186.

(58) Perdew, J. P.; Burke, K.; Ernzerhof, M. Generalized gradient approximation made simple. *Phys. Rev. Lett.* **1996**, *77*, 3865–3868.

(59) Grimme, S.; Antony, J.; Ehrlich, S.; Krieg, H. A consistent and accurate ab initio parametrization of density functional dispersion correction (DFT-D) for the 94 elements H-Pu. *J. Chem. Phys.* **2010**, *132*, 154104.

(60) Grimme, S.; Ehrlich, S.; Goerigk, L. Effect of the damping function in dispersion corrected density functional theory. *J. Comput. Chem.* **2011**, *32*, 1456–1465.

(61) Baskin, Y.; Meyer, L. Lattice constants of graphite at low temperatures. *Phys. Rev.* **1955**, *100*, 544–544.

(62) Huber, K.; Herzberg, G. *Constants of diatomic molecules. In: Molecular Spectra and Molecular Structure.*; Springer, Boston, MA, 1979.

(63) Ulbricht, H.; Zacharia, R.; Cindir, N.; Hertel, T. Thermal desorption of gases and solvents from graphite and carbon nanotube surfaces. *Carbon* **2006**, *44*, 2931 – 2942.

(64) Byrd, R. H.; Lu, P.; Nocedal, J.; Zhu, C. A limited memory algorithm for bound constrained optimization. *SIAM J. Sci. Comput.* **1995**, *16*, 1190–1208.

(65) Shen, X. J.; Lozano, A.; Dong, W.; Busnengo, H. F.; Yan, X. H. Towards Bond Selective Chemistry from First Principles: Methane on Metal Surfaces. *Phys. Rev. Lett.* **2014**, *112*, 046101.

(66) Moiraghi, R.; Lozano, A.; Busnengo, H. F. Theoretical Study of the Dissociative Adsorption of Methane on Ir(111): The Role of Steps and Surface Distortions at High Temperatures. *J. Phys. Chem. C* **2016**, *120*, 3946–3954.

(67) Seminara, G. N.; Peludhero, I. F.; Dong, W.; Martínez, A. E.; Busnengo, H. F. Molecular Dynamics Study of Molecular and Dissociative Adsorption Using System-Specific Force Fields Based on Ab Initio Calculations: CO/Cu(110) and CH_4/Pt(110). *Top Catal* **2019**, *62*, 1044–1052.

(68) Nosé, S. A unified formulation of the constant temperature molecular dynamics methods. *J. Chem. Phys.* **1984**, *81*, 511–519.

(69) Hoover, W. G. Canonical dynamics: Equilibrium phase-space distributions. *Phys. Rev. A* **1985**, *31*, 1695–1697.

(70) Groß, A.; Dianat, A. Hydrogen dissociation dynamics on precovered Pd surfaces: Langmuir is still right. *Phys. Rev. Lett.* **2007**, *98*, 206107.

(71) Nattino, F.; Díaz, C.; Jackson, B.; Kroes, G.-J. Effect of surface motion on the rotational quadrupole alignment parameter of D_2 reacting on Cu(111). *Phys. Rev. Lett.* **2012**, *108*, 236104.

(72) Nattino, F.; Ueta, H.; Chadwick, H.; van Reijzen, M. E.; Beck, R. D.; Jackson, B.; van Hemert, M. C.; Kroes, G.-J. Ab Initio molecular dynamics calculations versus quantum-state-resolved experiments on CHD_3 + Pt(111): New insights into a prototypical gas surface reaction. *J. Phys. Chem. Lett.* **2014**, *5*, 1294–1299.

(73) Kolb, B.; Guo, H. Communication: Energy transfer and reaction dynamics for DCl scattering on Au(111): An ab initio molecular dynamics study. *J. Chem. Phys.* **2016**, *145*, 011102.

(74) Novko, D.; Lončarić, I.; Blanco-Rey, M.; Juaristi, J. I.; Alducin, M. Energy loss and surface temperature effects in ab initio molecular dynamics simulations: N adsorption on Ag(111) as a case study. *Phys. Rev. B* **2017**, *96*, 085437.

(75) Zhou, X.; Kolb, B.; Luo, X.; Guo, H.; Jiang, B. Ab Initio molecular dynamics study of dissociative chemisorption and scattering of CO_2 on Ni(100): Reactivity, energy transfer, steering dynamics, and lattice effects. *J. Phys. Chem. C* **2017**, *121*, 5594–5602.

(76) Zhou, L.; Jiang, B.; Alducin, M.; Guo, H. Communication: Fingerprints of reaction mechanisms in product distributions: Eley-Rideal-type reactions between D and CD_3/Cu(111). *J. Chem. Phys.* **2018**, *149*, 031101.

(77) Füchsel, G.; Zhou, X.; Jiang, B.; Juaristi, J. I.; Alducin, M.; Guo, H.; Kroes, G.-J. Reactive and nonreactive scattering of HCl from Au(111): An ab initio molecular dynamics study. *J. Phys. Chem. C* **2019**, *123*, 2287–2299.

(78) Billing, G. D. *Dynamics of Molecule Surface Interaction*; John Wiley & Sons, 2000.

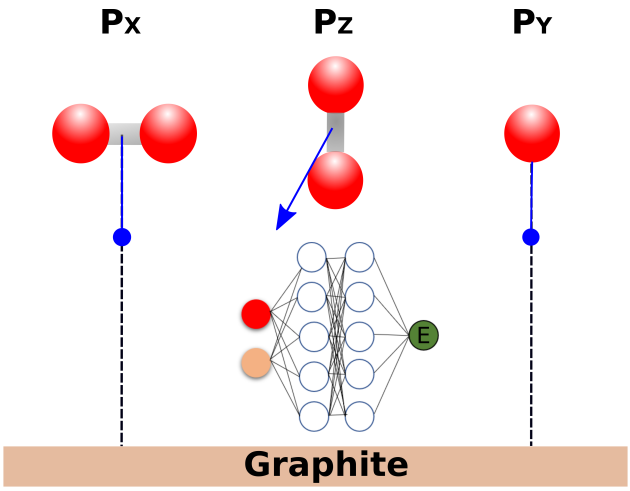

Figure 12: TOC Graphic